

Architected metamaterials with tailored 3D buckling mechanisms at the microscale

Zacharias Vangelatos^{a,b}, Grace X. Gu^{a,c}, Costas P. Grigoropoulos^{a,b,*}

^a Department of Mechanical Engineering, University of California, Berkeley, CA 94720, USA

^b Laser Thermal Laboratory, Department of Mechanical Engineering, University of California, Berkeley, CA 94720, USA

^c Gu Research Group, Department of Mechanical Engineering, University of California, Berkeley, CA 94720, USA



ARTICLE INFO

Article history:

Received 20 June 2019

Received in revised form 19 September 2019

Accepted 29 September 2019

Available online 8 October 2019

Keywords:

3D buckling

Microlattice structures

Multi-photon absorption

ABSTRACT

Attaining architected structures with unprecedented properties not found in natural materials is a long-sought goal for both materials science and additive manufacturing. Improving the mechanical behavior of engineered materials such as auxetics for bioengineering applications or bistable structures for mechanical actuation depends on the buckling mechanisms governing their response. Despite the fact that the design principles for two-dimensional buckling have been elucidated in previous studies, comprehending three dimensional buckling mechanisms is still tenuous. In this study, we aim to illuminate the buckling mechanisms governing the response of three-dimensional structures at the microscale, providing the critical guidelines for the design of novel metamaterials. In addition, finite element analysis and in-situ SEM – microindentation experiments are performed to investigate how scale effects affect the design principles to architect a controlled 3D buckling mechanism and reflect the mechanical response to the deformation of the structure in-situ. Our findings elicit the design process of tailored three dimensional buckling structures based on the geometric architecture instead of the behavior of the bulk material, while setting a broader framework to fabricate and characterize these structures at the microscale.

© 2019 Elsevier Ltd. All rights reserved.

1. Introduction

The design of architected materials has captured the attention of the research community for their extraordinary properties. The endeavor to merge the theoretical design of mechanical metamaterials [1] with the advances in additive manufacturing [2] and optimization [3,4] has provided a nexus between theoretical design of metamaterials and engineering applications. Designs such as ultralight-ultrastiff structures [5,6] provide high energy dissipation and strength, while auxetic materials provide high resilience to large deformations [6]. The mechanical response of these structures is determined by the buckling mechanisms dictating their behavior [7]. Buckling can be considered a dichotomous mechanism, as it can either be the cause of mechanical failure for conventional structural designs such as bridges [8] or it can provide unprecedented properties, such as in MEMS microstructures [9]. Buckling has been investigated for the case of two-dimensional geometries [10–14], furnishing the vast expansion of the design space. However, for three-dimensional

structures [15–17], the design principles have not been examined thoroughly to establish a coherent framework associated with the buckling behavior. The reason is that obtaining analytical solutions for large and nonlinear deformations is significantly arduous for the case of complex 3D geometries. Consequently, the evaluation of the mechanical response of 3D architected metamaterials has been limited to the control of the relative density of the structure [5,6,15,17], without utilizing analytical solutions for the deformation and stress fields. Hence, the design of three-dimensional controlled buckling is fairly empirical and the design space is comprised of a limited number of structures [18]. The primary objective for efficient design is to forestall out of plane buckling in the structure, which for the case of multi-layered structures results in “sliding” of some layers with respect to the others. Alternatively, internal buckling of the lattice members of the layer without out of plane deformation of the whole layer can lead to a functional mechanical response. These distinct buckling responses will be examined in the present work. The desired buckling behavior for high energy dissipation and reversible large deformations must institute a bistable mechanism in the structure. Bistability provides multiple local equilibrium states due to snap through buckling, which enables mechanical energy absorption and release without the requirement of perpetual actuation [7,19–22]. This structural principle has been utilized

* Corresponding author at: Department of Mechanical Engineering, University of California, Berkeley, CA 94720, USA.

E-mail addresses: zacharias_vangelatos@berkeley.edu (Z. Vangelatos), ggu@berkeley.edu (G.X. Gu), cgrigoro@berkeley.edu (C.P. Grigoropoulos).

for a plethora of applications, such as controlled wave propagation [22], soft robotics [23] and malleable structures [21]. The objective of this study is to investigate how out of plane buckling can be prevented and instead utilize a bistable mechanism and internal buckling of beam members of each layer. To instantiate this principle, a specially architected structure was designed, and its scale and size effects were investigated with respect to the buckling performance. The simplicity of this design aims to elucidate how complex 3D structures must be architected and which buckling modes, functional or egregious, can occur. These structures were fabricated by multiphoton lithography (MPL). Multiphoton lithography is the predominant fabrication technique to design complex geometries in nanoscale and microscale [24]. Structural features in these length scales have proved to be critical for the enhanced performance of patterns observed in nature, like seashells and bones [25]. Nature is the most articulated paradigm of design efficiency and hierarchical convoluted structures manifesting the mechanical principles of tailored buckling [26]. Thus far, snap through buckling and bistability are controlled utilizing slender members and elastomer materials [27]. Hence, the mechanical response is substantiated by the properties of the material for a very specific geometric design. Our proposed design renders the geometric features paramount, as elastomeric polymers are feeble to be utilized for very small length scales that require different materials for the fabrication process [9,24].

2. Design of controlled buckling structures

The design of the unit cell is delineated in Fig. 1A–B. The unit cell is bifurcated into two main beam members (colored red and blue). The blue members under compression or extension, as it is illustrated in Fig. 1C–D, will facilitate a snap through buckling mechanism due to a pre-existing bent angle of 150° .

During compression, these beam members will come in contact [28], increasing the stiffness of the structure and reemerging from the local minimum at the force displacement curve which was reached during the snap through mechanism [29]. Nevertheless, as it will be shown later, these members cannot hinder out of plane buckling, which will be proved to depend on scale effects. Hence, another set of members was included in the unit cell to enhance the structural stability and provide an extra snap through mechanism (colored red). The assembly of the unit cells for the design of a complex structure is depicted in Fig. 1E. The secondary members were positioned such that they will not encounter the primary members during the deformation, thereby maligning the final performance of the structure. All members are connected with a hexagonal base (colored gray) to assemble the unit cells at different layers (Fig. 1E). Moreover, they will also buckle during the deformation, enhancing the energy dissipation of the structure.

To validate the feasibility of the designed structure, finite element analysis (FEA) simulations were performed. Further details about the simulations are provided in the supplementary information. The buckling mechanism of the structure is determined by the following equation:

$$\{[\mathbf{K}_o] + [\mathbf{K}_u] + N[\mathbf{K}_\sigma]\} d\mathbf{u} = d\mathbf{q} \quad (1)$$

where $[\mathbf{K}_o]$ is the linear stiffness matrix, $[\mathbf{K}_u]$ is the initial displacement stiffness matrix and $[\mathbf{K}_\sigma]$ is the initial stress stiffness matrix. N is the internal loading applied to the structure, while $d\mathbf{u}$ is the incremental displacement of the structure for external load $d\mathbf{q}$. For the case of one-dimensional problems, buckling occurs when the structure deforms in a direction that there is no loading and the stiffness becomes negative, leading to a state of structural instability. For the three-dimensional case this mechanism is

manifested when $d\mathbf{u}$ is not equal to zero, while there is no external load $d\mathbf{q}$. Then, the stiffness becomes positive semidefinite and the structure will teeter. For small incremental deformations, neglecting the contribution of $[\mathbf{K}_u]$, this corresponds to the following eigenvalue problem

$$\det \{[\mathbf{K}_o] + N_B[\mathbf{K}_\sigma]\} d\mathbf{u}_B = 0 \quad (2)$$

At this state, N_B is the value of the load that will initiate buckling, and $d\mathbf{u}_B$ is the characteristic buckling deformation, which corresponds to the eigenvector of N_B . The objective is to tailor the value of $d\mathbf{u}_B$, prohibiting out of plane buckling and instead enabling a mechanism that transfers the deformation to subsequent unit cells in a manner similar to stable wave propagation [22], one of the primary applications of tailored buckling. To analyze how the dimensions and the number of unit cells affect the characteristic buckling deformation, the FEA was performed for four different cases. The classical theory of structural buckling addresses how the dimensions of beam members affect the buckling load by the following relation $N_B \sim \frac{EI}{(L_{\text{eff}})^2}$ where E is the Young's modulus, I is the inertia of the structure, which is a function of the cross section dimensions and L_{eff} is the effective length of the beam based on its boundary conditions [2]. Nevertheless, there is no formulation how the characteristic buckling deformation is affected by the dimensions of the structures. Therefore, the design principle must focus on how $d\mathbf{u}_B$ can be tailored as a function of the height and thickness of the members, considering the fabrication capabilities that are required.

3. Results

3.1. Finite element simulations of the architected structures

Characteristic examined structures demonstrating the distinct mechanical responses that can be attained are presented in Fig. 2A–D. The unit cell height h over the beam member diameter d for every case is $h/d = 12, 36, 12$ and 14.4 for ten, seven, seven and three unit cells on each layer respectively. These dimensions were selected such that the structures with the slenderest members can preserve their structural integrity under their own weight and not collapse during the fabrication process. The number and orientation of the unit cells were selected to provide symmetry in the 2D space, halting tendency for out of plane buckling. It must be noted that the mechanical response will be affected by the number of the unit cells on the structure until a specific number of unit cells, for which it will be uniform. For the presented designs, we assembled the minimum number of unit cells required to observe the behavior of a uniform material without early fracture of the individual unit cells. Furthermore, functional structures require more than one unit cell, taking into account the provided manufacturing techniques to fabricate them. The static deformations under compression for each design are illustrated in Fig. 2E–H.

For every design, the primary members come to close proximity, enabling post contact that reverses the negative stiffness of the structure due to buckling. The members positioned at the center mitigate the total compression, providing a threshold for structural integrity and hindering catastrophic failure. However, the height of the first structure is low relative to the deformation that can be applied, resulting the members that deform to come in contact for the case of large deformations, mitigating the buckling instability mechanism and increasing the intrinsic stiffness of the structure. The eigenvalue buckling analysis characteristic deformations are presented in Fig. 2I–L. For the ratios equal to 12 (Figs. 2I and 2K), the desired eigenvectors $d\mathbf{u}_B$ are achieved, providing the buckling of the internal members and preventing out of plane buckling, which occurs for the ratios 36 and 14.4

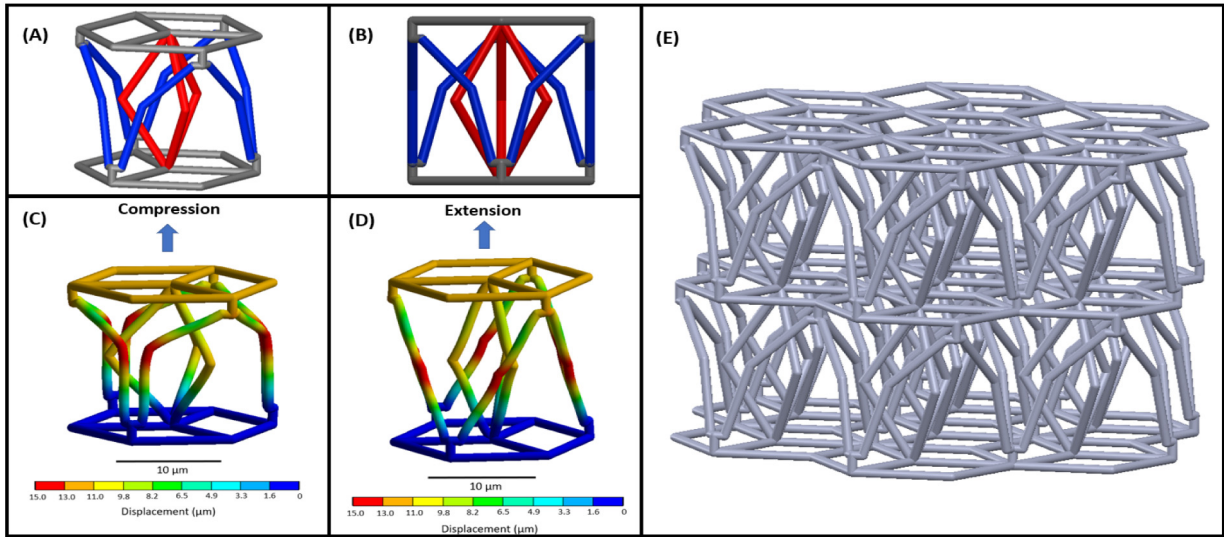


Fig. 1. The proposed designed structure. (A) Isometric view of the designed structure. (B) Side view of the unit cell. The external beam members (colored blue) provide the primary buckling members, while the main purpose of the internal ones (colored red) is to provide structural integrity for the unit cell. (C–D) The mechanical response of the unit cell under compression and extension by FEA analysis. (E) Assembly of unit cells to form a periodic structure.

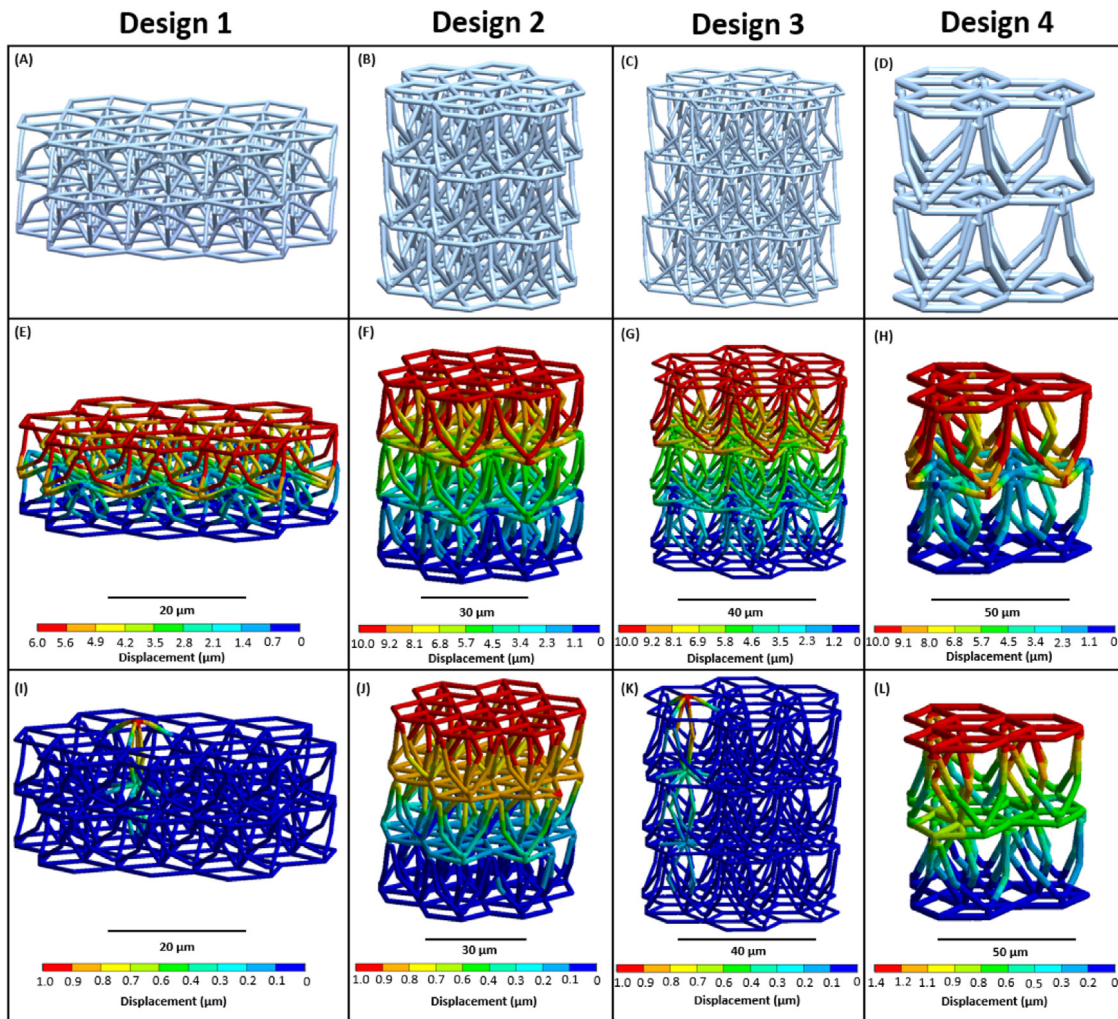


Fig. 2. FEA analysis for the structural behavior and eigenvalue buckling analysis of the designed structures. (A–D) Final structures for different height/diameter ratios. (E–H) FEA static analysis for every structure illustrating the points of potential failure under compression and how post contact will occur. (I–L) The characteristic buckling deformation du_B for all structures, indicating how buckling will commence when the critical load N_B is reached.

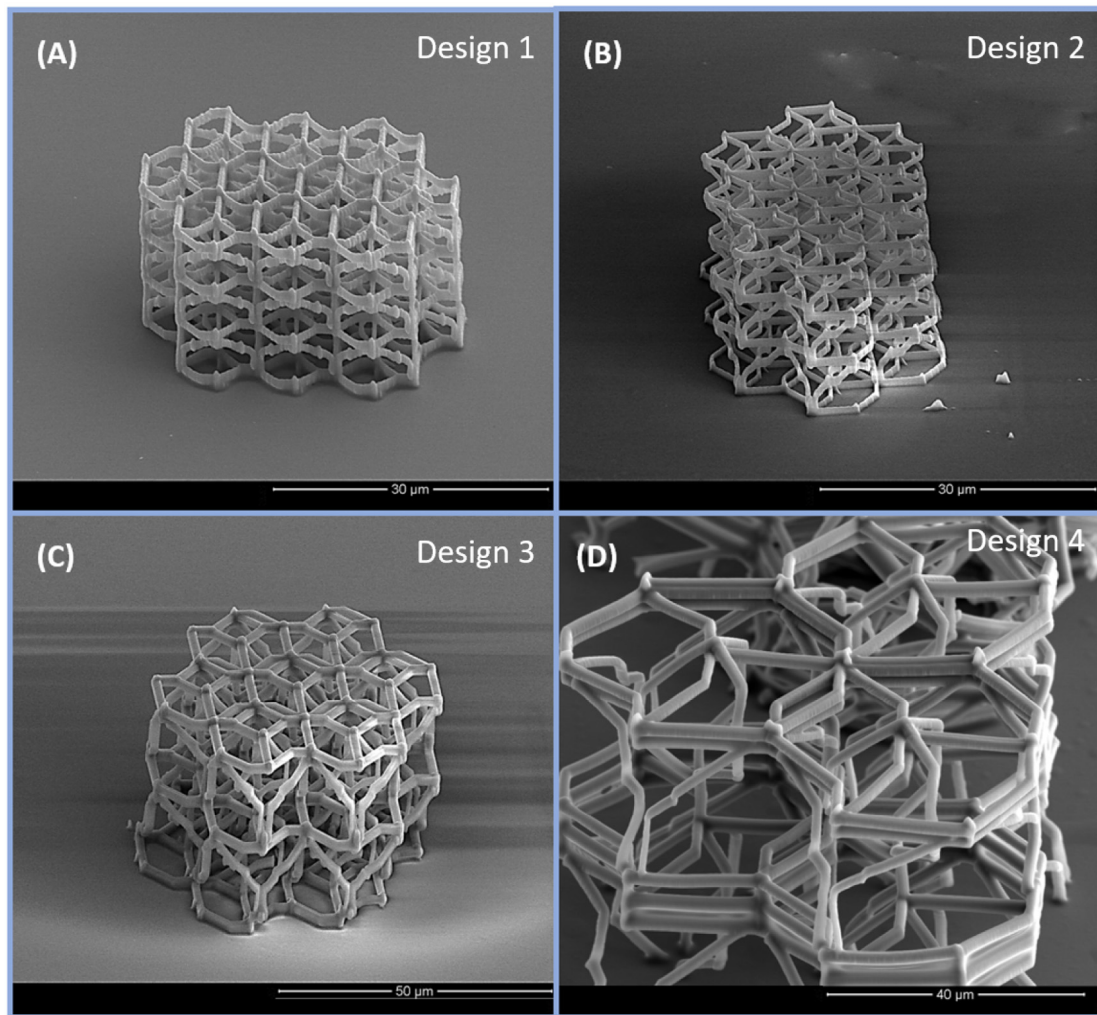


Fig. 3. The fabricated structures. (A) Design 1 with unit cell height $6\ \mu\text{m}$ and beam diameter $0.5\ \mu\text{m}$. (B) Design 2 with unit cell height $18\ \mu\text{m}$ and beam diameter $1.5\ \mu\text{m}$. (C) Design 3 with unit cell height $18\ \mu\text{m}$ and beam diameter $0.5\ \mu\text{m}$. (D) Design 4 with unit cell height $36\ \mu\text{m}$ and beam diameter $2.5\ \mu\text{m}$. The maximum number of unit cells of each design was utilized to fabricate the largest periodic structure, based on the workspace of the setup.

(Figs. 2J and 2L). For these designs, the internal buckling of the beam members is not obtained and instead the whole structure deforms in a direction different from that of the load (i.e. in the lateral direction of the geometry).

3.2. Fabrication and mechanical response of the architected structures

To validate the simulations results, the structures were fabricated by MPL. Further details about the experimental apparatus and the materials are provided elsewhere [24]. The fabricated structures with the same dimensions as in the simulations are presented in Fig. 3. The high spatial resolution of MPL enables a truly 3D fabrication process, unbound or layer-by-layer constraints of other fabrication processes such as microstereolithography [1]. The mechanical behavior of the fabricated metamaterial structures was examined with a nanoindentation apparatus, assembled inside a Scanning Electron Microscope for in-situ recording of the deformation. Details about the experimental procedure are provided in the supplementary information.

Characteristic force displacement curves for each structure are presented in Figs. 4 and 5. Each curve is collated with the in-situ imaging of the deformed structure to interpret the mechanical response. The first structure has a response that can be distinguished in three stages (SI Movie1). From the undeformed

configuration (stage A in Fig. 4A) the structure is loaded until the slope becomes negative (stage B), indicating the initiation of buckling, which occurs at $251.1\ \mu\text{N}$. As the buckled members have sustained large deformations, they encounter the neighboring ones (as it is observed from the SEM imaging on stage B of Fig. 4A). This post contact causes an immediate intrinsic stiffening mechanism, making the slope positive again until the structure is unloaded (stage C). For this length scale the result is consistent with the FEA, as instability occurs without out of plane buckling. Nonetheless, the distance between the members is small for a large compression, causing the members to encounter the structure instantaneously after buckling, mitigating instability. Regarding the second design (Fig. 4 B) there is a tripartite mechanical response as well (SI Movie2). However, as the structure deforms (stage A), out of plane buckling commences at $209.6\ \mu\text{N}$, a result consonant with the FEA analysis. The corollary is the denigration of the structure's performance, as after unloading the structure has collapsed irreversibly (stage C of Fig. 4B). The third design's response (Fig. 5A) has five stages (SI Movie3). The scale factor for this design is the same as the first structure, and the buckling mechanism is evinced at $551.5\ \mu\text{N}$ (stage B on Fig. 5A). In addition, the higher height of the unit cell enables the secondary members and the base to buckle as well before approaching each other, inaugurating two more buckling mechanisms at $565.7\ \mu\text{N}$ and $571.8\ \mu\text{N}$ (stages C and D), until it

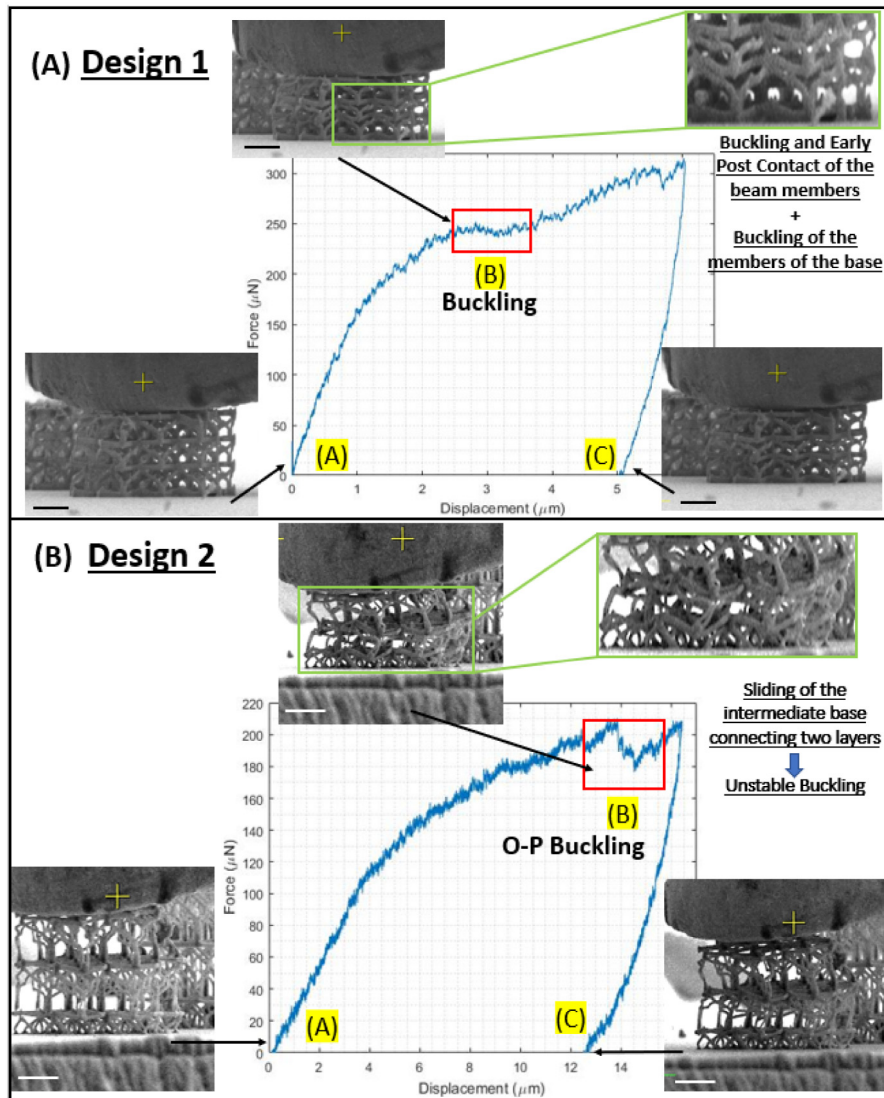


Fig. 4. In situ SEM — Microindentation tests for designs 1 and 2. (A) Force displacement curve for Design 1. Buckling commences on the designated stage, but the post contact of the beam members due to small height of the unit cells decrease its effect. (B) Force displacement curve for Design 2. For this case out of plane (O-P) buckling occurs, as the slender lattice members cannot provide the required stability to prevent the intermediate base from out of plane buckling. Black length scale bar = $10 \mu\text{m}$ and white length scale bar = $20 \mu\text{m}$.

is unloaded (stage E). The fourth structure (SI Movie4) proved to be the most volatile (Fig. 5B) as the increased height of the unit cells combined with the slender members resulted in bending of the members and a barrel shape deformed configuration, as it is depicted on stage B. Nevertheless, buckling did not occur, and the mechanical response was not the desired one.

4. Discussion and conclusions

Juxtaposing the FEA with the indentation experiments, the buckling mechanism was efficiently demonstrated for the ratio equal to 12, while for the 36 out of plane buckling occurred, and for 14.4 structural failure commenced. Tacitly, tuning the member slenderness will cause structural instability at lower loads. Nevertheless, the structure does not have the proclivity to buckle towards the lower layer of the structure, as it was presented in Figs. 4B and 5B. Even though members with larger cross sections are less unstable, the inherent higher volume of the material provides the heterodox advantage of the enhanced resilience of the structure to out of plane buckling, while enabling the desired large deformation propagation to subsequent layers.

Furthermore, the relative orientation of the beam is crucial for efficient designs. Post contact of the buckled members will provide the positive slope to be rejuvenated again, returning the structure to its stable state. However, for short unit cells, the buckled elements come into contact too fast and the buckling behavior cannot be utilized efficiently. The third structure proved to have the correct combination of height and thickness such that the snap through buckling mechanism is observed and the post contact does not occur instantly after buckling. This design provides the perforation for the materialization of buckling on different sections of the unit cells. Hence, at this scaling factor, the designed structure conflates the multistability and the structural integrity that is required for a functional design.

In summary, we demonstrated a novel architected structure tailoring the buckling mechanism in three dimensional space for a functional multistable material. The objective was to comprehend how different buckling modes and mechanical responses can commence at the same 3D structure for different length-scales. The structural principle governing the system was based on a buckling mechanism coalesced with the post contact of the structural members, providing the undulated profile on the

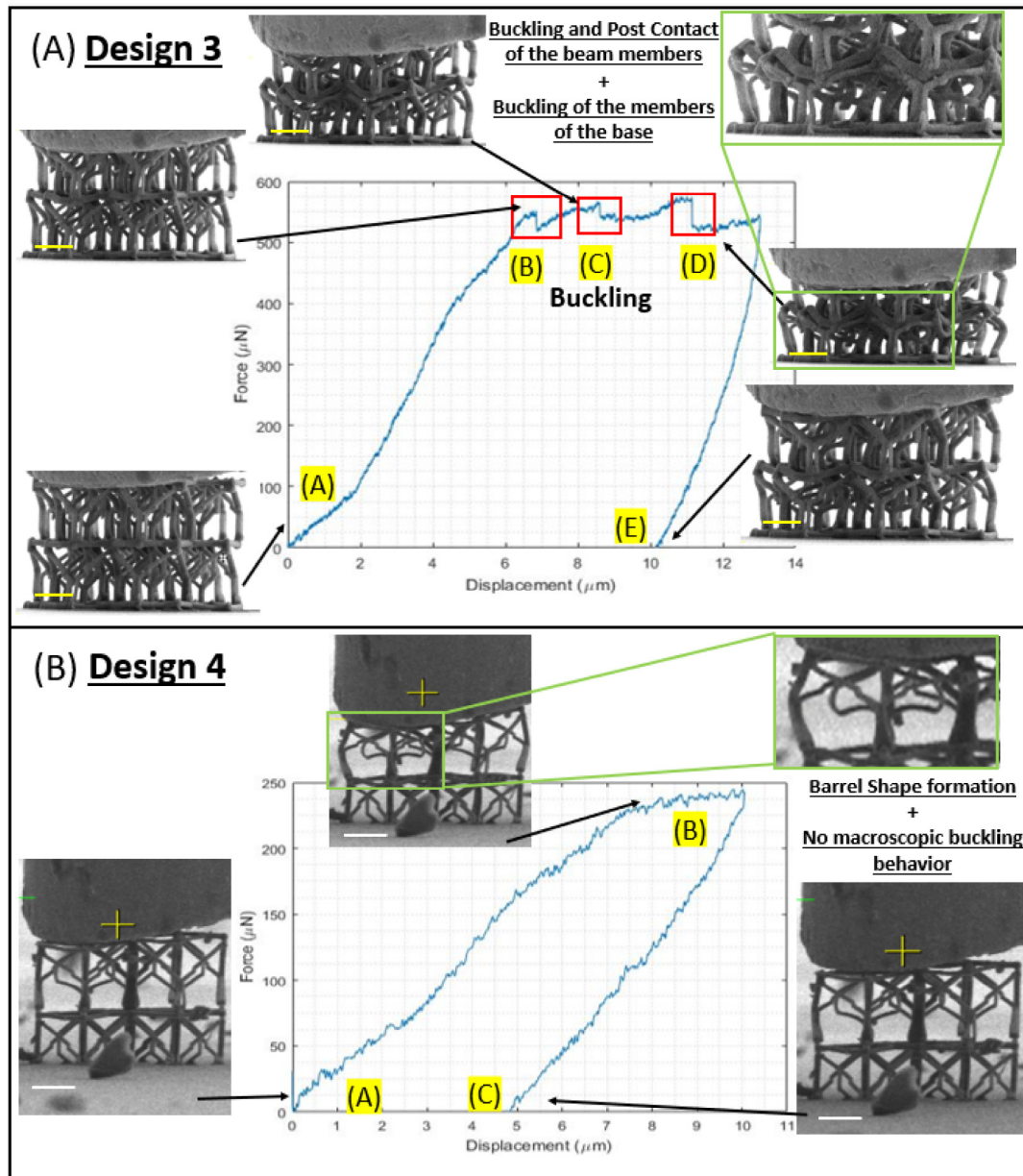


Fig. 5. In situ SEM – Microindentation tests for designs 2 and 3. (A) Force displacement curve for Design 3. For these dimensions the structure exhibits the desired behavior. The structure is subject to internal buckling and the larger distance between the lattice members provides a multistable response. (B) Force displacement curve for Design 4. The increased height and slender lattice members render the structure non-functional, due to the barrel shape formation during compression. Yellow length scale bar = 15 μm and white length scale bar = 35 μm .

force displacement curves during snap through buckling. Utilizing simple lattice elements, we accomplished designing a structure that can facilitate buckling based on its geometric configuration. Both the FEA analysis and the microindentation experiments for different length scales provided an insight for the dimensions that manifest internal buckling on the structure rather than out of plane buckling. The simplicity of the design enables the scalability of the structure for applications including robotic actuation [23]. Nevertheless, microscale buckling structures are also imperative for tissue engineering and controlled muscle suspension [30]. Finally, a systematic approach must be addressed to formulate the vector space of the buckling eigenvectors as a function of the unit cell geometric parameters. For this purpose, optimization techniques such as machine learning [31,32] could be utilized to relate these quantities instead of analytical solutions. This approach will pave the way for the expansion of the design space

with more three-dimensional structures that can utilize tailored buckling.

Declaration of competing interest

The authors declare that they have no known competing financial interests or personal relationships that could have appeared to influence the work reported in this paper.

Acknowledgments

This work was supported by the National Science Foundation (NSF), United States under the Scalable Nanomanufacturing (SNM) Program, Award No. 1449305. The authors thank Professor Peter Hosemann, Department of Nuclear Engineering, University

of California, Berkeley, for the use of the microindentation apparatus. The MPL setup and software were built by I. Sakellari and A. Lemonis of IESL/FORTH, respectively.

Appendix A. Supplementary data

Supplementary material related to this article can be found online at <https://doi.org/10.1016/j.eml.2019.100580>.

References

- [1] A.C. Fischer, M. Mäntysalo, F. Niklaus, Inkjet printing laser-based micro-machining and micro 3D printing technologies for MEMS, in: *Handbook of Silicon Based MEMS Materials and Technologies*, Chapter 26, 2015, pp. 550–564.
- [2] M.F. Ashby, The properties of foams and lattices, *Phil. Trans. R. Soc. A* 364 (2006) 15–30.
- [3] G.X. Gu, C. Chen, D.J. Richmond, M.J. Buehler, Bioinspired hierarchical composite design using machine learning: simulation, additive manufacturing, and experiment, *Mater. Horiz.* 5 (2018) 939.
- [4] G.X. Gu, M. Takaffoli, M.J. Buehler, Hierarchically enhanced impact resistance of bioinspired composites, *Adv. Mater.* 29 (2017) 1700060.
- [5] L.R. Meza, S. Das, J.R. Greer, Strong, lightweight, and recoverable three-dimensional ceramic nanolattices, *Science* 345 (2014) 1322–1326.
- [6] S. Babae, J. Shim, J.C. Weaver, E.R. Chen, N. Patel, K. Bertoldi, 3D soft metamaterials with negative Poisson's ratio, *Adv. Mater.* 25 (2013) 5044–5049.
- [7] K. Bertoldi, V. Vitelli, J. Christensen, M. van Hecke, Flexible mechanical metamaterials, *Nat. Rev. Mater.* 2 (2017) 17066.
- [8] A.S. Vlahinos, J.Ch. Ermopoulos, Y.-C. Wang, J buckling analysis of steel arch bridges, *Construct. Steel Res.* 26 (1993) 59–71.
- [9] R.K. Jayne, T.J. Stark, J.B. Reeves, D.J. Bishop, A.E. White, Dynamic actuation of soft 3D micromechanical structures using micro-electromechanical systems (MEMS) adv, *Mater. Technol.* 3 (2018) 1700293.
- [10] D. Restrepo, N.D. Mankame, P.D. Zavattieri, Phase transforming cellular materials, *Extreme Mech. Lett.* 4 (2015) 52–60.
- [11] C. Findeisen, J. Hohe, M. Kadic, P. Gumbsch, Characteristics of mechanical metamaterials based on buckling elements, *J. Mech. Phys. Solids* 102 (2017) 151–164.
- [12] K. Che, C. Yuan, J. Wu, H.J. Qi, J. Meaud, Three-dimensional-printed multistable mechanical metamaterials with a deterministic deformation sequence, *J. Appl. Mech.* 84 (2016) 011004.
- [13] S. Shan, S.H. Kang, J.R. Raney, P. Wang, L. Fang, F. Candido, J.A. Lewis, K. Bertoldi, Architected materials for trapping elastic strain energy, *Adv. Mater.* 27 (2015) 4296–4301.
- [14] Q. Chen, X. Zhang, B. Zhu, Multistable design of buckling-induced mechanical metamaterials for energy absorption using topology optimization, *Struct. Multidiscip. Optim.* 58 (2018) 1395–1410.
- [15] J. Xiao, Y. Chen, X. Lu, B. Xu, X. Chen, J. Xu, Three dimensional buckling beam under cylindrical constraint, *Int. J. Mech. Sci.* 150 (2019) 348–355.
- [16] J. Bauera, S. Hengsbach, I. Tesari, R. Schwaiger, Oliver Kraft, High-strength cellular ceramic composites with 3D microarchitecture, *Proc. Natl. Acad. Sci. USA* 111 (2014) 2453–2458.
- [17] P. Hyman, A.I. Osofero, S. Sriramula, Buckling behaviour of three-dimensional prestressed stayed columns, *IOP Conf. Ser.: Mater. Sci. Eng.* 413 (2018) 012007.
- [18] J. Paulose, A.S. Meeussen, V. Vitelli, Buckling behaviour of three-dimensional prestressed stayed columns, *Proc. Natl. Acad. Sci. USA* 112 (2015) 7639–7644.
- [19] H. Yang, L. Ma, Multi-stable mechanical metamaterials with shape-reconfiguration and zero Poisson's ratio, *Mater. Des.* 152 (2018) 181–190.
- [20] H. Yang, L. Ma, Multi-stable mechanical metamaterials by elastic buckling instability, *J. Mater. Sci.* 54 (2019) 3509–3526.
- [21] B. Haghpanah, L. Salari-Sharif, P. Pourrajab, J. Hopkins, L. Valdevit, Multistable shape-reconfigurable architected materials, *Adv. Mater.* 28 (2016) 7915–7920.
- [22] J.R. Raney, b. N. Nadkarnic, C. Daraiod, D.M. Kochmann, J.A. Lewis, K. Bertoldi, Multistable shape-reconfigurable architected materials, *Proc. Natl. Acad. Sci. USA* 113 (2016) 9722–9727.
- [23] T. Chen, O.R. Bilal, K. Shea, C. Daraio, Harnessing bistability for directional propulsion of soft untethered robots, *Proc. Natl. Acad. Sci.* 115 (2018) 5698–5702.
- [24] I. Sakellari, E. Kabouraki, D. Gray, V. Purlys, C. Fotakis, A. Pikulin, N. Bityurin, M. Vamvakaki, M. Farsari, Diffusion-assisted high-resolution direct femtosecond laser writing, *ACS Nano* 6 (2012) 2302–2311.
- [25] H. Gao, B. Ji, I.L. Jäger, E. Arzt, P. Fratzl, Materials become insensitive to flaws at nanoscale: Lessons from nature, *Proc. Natl. Acad. Sci. USA* 100 (2003) 5597–5600.
- [26] A.M. Merzer, R. Freund, Buckling of strike-slip faults—in a model and in nature, *Geophys. J. R. Soc.* 43 (1975) 517–530.
- [27] A. Rafsanjani, A. Akbarzadeh, D. Pasini, Snapping mechanical metamaterials under tension, *Adv. Mater.* 27 (2015) 5931–5935.
- [28] N. Adan, I. Sheinman, E. Altus, Post-buckling behavior of beams under contact constraints, *J. Appl. Mech.* 61 (1994) 764–772.
- [29] M.F. Berwind, A. Kamas, C. Eberl, A hierarchical programmable mechanical metamaterial unit cell showing metastable shape memory, *Adv. Eng. Mater.* 20 (2018) 1800771.
- [30] F.S.L. Bobbert, S. Janbaz, A.A. Zadpoor, Towards deployable meta-implants, *J. Mater. Chem. B* 6 (2018) 3449–3455.
- [31] C. Chen, G.X. Gu, Effect of constituent materials on composite performance: Exploring design strategies via machine learning, *Adv. Theory Simul.* (2019) 1900056.
- [32] C. Chen, G. Gu, Machine learning for composite materials, *MRS Commun.* (2019) 1–11.